analytica

MDPI

Article

Role of a Drastic Mechanical Treatment Toward Improving the Electrochemical Performance of a Solid-Gold Electrode

Paolo Inaudi [1,*], Gabriele Ruggieri [2], Elena Orrù [3], Ornella Abollino [1], Agnese Giacomino [1], Letizia Mazzoni [1], Mery Malandrino [2] and Francesca Durbiano [4]

[1] Department of Drug Science and Technology, University of Torino, Via Pietro Giuria 9, 10125 Turin, Italy; ornella.abollino@unito.it (O.A.); agnese.giacomino@unito.it (A.G.); letizia.mazzoni@unito.it (L.M.)
[2] Department of Chemistry, University of Torino, Via Pietro Giuria 7, 10125 Torino, Italy; gabr.ruggieri@gmail.com (G.R.); mery.malandrino@unito.it (M.M.)
[3] Lavazza S.p.A., Via Bologna 32, 10152 Torino, Italy; elena.orru@lavazza.com
[4] INRiM, Istituto Nazionale di Ricerca Metrologica, Strada delle Cacce 91, 10135 Torino, Italy; f.durbiano@inrim.it
* Correspondence: paolo.inaudi@unito.it

Abstract

A simple mechanical polishing treatment of commercial solid-gold electrodes (SGEs) can renew the active gold surface, reduce manufacturing-related grooves, and markedly improve the repeatability of geometric-area estimation and the analytical performance in stripping voltammetry. The work focuses on the accurate determination of the geometric area of a SGE by two voltammetric techniques. Cyclic voltammetry (CV) at different scan rates, referred to as the Randles–Ševčik equation, and voltage scans at different electrode rotation rates, based on the Levich equation, were performed. The geometric area of the SGE was also evaluated by scanning electron microscopy (SEM). Commercial SGEs show grooves on their surface, derived from the fabrication processes. The effects of these grooves on the voltammetric response were investigated. The measurements were carried out on the SGE both as received from the manufacturer and after a reduction in the grooves height by a drastic mechanical treatment. After the treatment, the estimated area values were lower and more precise (3.05 ± 0.02 mm^2). Moreover, the reduction in the grooves' height affected the area estimations in contrast with the meaning of the geometric area, as intended by the Randles–Ševčik and Levich equations. Furthermore, the gold exposed surface was measured by CV in sulphuric acid. Finally, the SGE was tested for the detection of Hg in a NaCl solution by anodic stripping voltammetry: the repeatability of the response improved after the mechanical treatment, confirming the usefulness of this step before electrode usage.

Keywords: electrode area determination; solid-gold electrode; geometric area; Randles–Ševčik equation; Levich equation

Check for updates

Academic Editor: Simone Morais

Received: 22 December 2025
Revised: 29 January 2026
Accepted: 11 February 2026
Published: 13 February 2026

Copyright: © 2026 by the authors. Licensee MDPI, Basel, Switzerland. This article is an open access article distributed under the terms and conditions of the Creative Commons Attribution (CC BY) license.

1. Introduction

For many years mercury electrodes have been the transducers of choice of several analytes in most voltammetric techniques, and in particular stripping voltammetry thanks to their high sensitivity, reproducibility and linearity. However, due to the toxicity of mercury, in recent decades these electrodes have been scarcely used in the analytical practice and excluded from the out-of-laboratory applications [1–3]. Other environmentally friendly electrode materials have become highly desired for both centralized and field

applications. In particular, solid-gold electrodes represent a very attractive alternative to mercury based electrodes, and, in addition, they can present much larger surface areas than that of mercury drop electrodes. Moreover, advances in technology and chemical procedures have provided new means for modifying their surface in a controlled way, thus increasing their selectivity and/or sensitivity [4–6].

In stripping voltammetry, electrodes of noble metals (platinum, palladium, and gold) are most frequently used for the detection of electropositive elements as As, Hg, Se, Cu, and Sb [7–10]. In addition, solid-gold [11–14] and gold-film electrodes [15,16], compared to the other noble metal electrodes, are able to achieve lower detection limits (at μg/L levels or below) for such analytes.

Electrode area determination is a crucial aspect to be accounted for in the electrochemical measurements, considering all the possible applications of the electrodes. However, in general, values obtained for a surface area depend on the method of measurement. Various in situ and ex situ experimental methods have been proposed for this aim, for example underpotential deposition of metals or porosimetry respectively [17]. Currently, a method widely applied in electrocatalysis for fuel cells and electrochemical capacitors for the estimation of the surface area involves the measurement of the amount of gas adsorbed on the solid surface at a temperature close to the boiling point of the gas [18]. Nitrogen, hydrogen and oxygen are the most commonly used as adsorbates [19–21]. However, the size of the adsorbate molecule (the probe molecule), the exposed crystallographic planes at the surface and the measurement temperature are parameters that affect the value of the surface area obtained.

Much attention has been paid to the characterization of the real surfaces using fractal geometry, which has played an important role in understanding the anomalous behavior of rough surfaces and interfaces [22,23].

However, a specific method to achieve a reliable estimation of the surface area has not yet been established. In general, each resulting surface area value depends on the dimension of the probe used, on the method of measurement and on the operative conditions adopted [24,25]. For these reasons, the most appropriate method for the surface area estimation was established to be the one which best approaches the experimental situation to which the value obtained has to be applied [17]. Moreover, attention has to be paid to the type of area which has to be determined. In fact it is possible to define two different types of area for a given electrode: (i) the geometric area, which is the cross-sectional area of the enclosure formed by projecting the boundary outward of the electrode in parallel with the surface normal, and (ii) the microscopic area, which considers the exposed surface and takes into account all the undulations, asperities and crevices present on it [17,26].

This work is focused on the proposal of a voltammetric technique for the assessment of the geometric area of a solid electrode to be used for voltammetric measurements. Specifically, a commercial solid-gold electrode (SGE) was chosen because it is frequently used in voltammetry for the determination of mercury [16]. It is easy to use, it has the possibility to be electrochemically and mechanically polished, it can be rotated during the measurement time and, since it exhibits a flat and planar macro-surface, mass transport of analyte can occur by diffusion [27].

For the estimation of the geometric area of the SGE, two voltammetric techniques, which operate in a steady-state voltammetry mode and in which the current is reported as a function of experimentally calculable parameters, were investigated: cyclic voltammetry (CV) at different scan rates, referred to the Randles–Ševčik equation [26], and linear scan voltammetry (LSV) at different electrode rotation rates, based on the Levich equation [28]. These equations are well known in electrochemistry and express the current produced by the reaction of the analyte occurring at the electrode in terms of different parameters,

including the geometric area of the electrode [26,27,29]. This geometric area approach is justified by the fact that for these two voltammetric techniques the steady state current is achieved, and the mass transport is controlled by diffusion, rather than by reaction kinetics [30].

The well-known reversible redox reaction of ferrocene/ferrocenium was chosen as a pilot compound, since this species is expected to undergo a simple one-electron transfer reaction, straightforward by associated chemical processes [26].

In the first stage of the study, the SGE was used as received by the producer. Then, a drastic mechanical treatment (MT) was carried out in order to reduce the height of the grooves present on its surface.

A comparison of the geometric area values of the SGE, obtained by the two voltammetric techniques before and after this MT was carried out. Then the outcomes of voltammetry were compared with the area obtained by the elaboration of images taken by a scanning electron microscope (SEM).

The theoretical aspects, the mathematical calculations, and the findings raised during the experiments, are critically exposed and explained. Moreover, an advantage of the voltammetric techniques for the determination of the geometric area is that they can be performed during any electrochemical application [31].

In addition, the exposed surface of the SGE was determined by CV in sulphuric acid.

Finally, Hg detection by ASV was performed before and after the MT in order to verify its effect on the analytical response.

2. Materials and Methods

2.1. Materials

Analytical-grade reagents were used throughout. Solutions of 1×10^{-3} M ferrocene ($Fe(C_5H_5)_2$, Fluka, 98% purity) in acetonitrile (AN) and tetrabutylammonium hexafluorophosphate ($TBAPF_6$) in concentration of 1×10^{-1} M were employed to investigate the surface area of the SGE by CV and LSV. Ferrocene and $TBAPF_6$ were weighted keeping the variability of the respective masses within 1%. Fresh solutions were daily prepared to avoid their possible degradation.

Solutions of 0.5 M H_2SO_4 (Fluka, 99% purity) were used to activate and monitor the SGE and to evaluate its exposed surface.

Solutions of 1 μg/L of Hg(II) in 0.06 M NaCl (used as supporting electrolyte) were prepared by successive dilutions from a 1000 mg/L standard solution of mercury (Merck, Darmstadt, Germany) directly in the voltammetric cell.

High purity water obtained from a Milli-Q apparatus (Millipore, Bedford, MA, USA) was used throughout the experiments.

2.2. Techniques for the Determination of the Geometric Area of the SGE

All the procedures described here were performed for the determination of the geometric area of the SGE adopting the same conditions, before and after the MT described in Section 2.4.

2.2.1. Voltammetric Procedures

Voltammetric analyses were performed with a PGSTAT10 potentiostat (Eco Chemie, Utrecht, The Netherlands) coupled to a 663 VA Metrohm (Herisau, Switzerland). The potentiostat was interfaced to a personal computer; the operational conditions were selected and voltammograms were visualized and processed with GPES 4.9 software. A configuration of three electrodes was used: an Ag/AgCl/KCl (3M) (cod. 6.0728.010) coupled with the electrolyte vessel (cod. 6.1245.010) as a reference electrode (RE), a glassy carbon rod (cod.

6.1247.000) as an auxiliary electrode (AE), and the SGE (gold electrode tip, cod. 6.1204.140) as a working electrode (WE), all purchased from Metrohm. The SGE is encased in a rod of inert insulator with a gold disk exposed at one end. The diameter of the gold disk declared by the manufacturer was of 2.0 ± 0.1 mm. In this work the SGE was used both as a fixed and a rotating electrode. The potential was applied between the WE and the RE and the current was measured between WE and the AE during the potential scans.

A cleaning step was applied before each voltammetric measurement to remove impurities possibly deposited and to restore the initial measurement conditions. The cell and its attachments were filled with 20 mL of a solution composed of 0.1 M $HClO_4$, 1.5×10^{-3} M NaCl and 5×10^{-4} M $EDTANa_2$ and the WE was rotated for 60 s at 0.6 V.

Successively, 10 CV cycles in 0.5 M H_2SO_4 from 0 to 1.5 V were applied before each measurement to activate and monitor the SGE surface.

The temperature of the solutions was maintained at $T = 298 \pm 1$ K during the measurements.

Measurements by CV Varying the Scan Rate

The SGE was plunged into a stagnant sample of the ferrocene solution described in Section 2.1. CV was applied and potential was varied linearly from 0 V to 0.85 V and ramped back to 0 V. Step potential was maintained at 0.00244 V. Eight values of scan rate, namely 10, 25, 50, 100, 200, 300, 400 and 500 mV/s were selected. After each scan, the solution was stirred to supply the electrode surface with fresh analyte. For each selected scan rate, a voltammogram was obtained and the anodic peak current was measured in automatic mode. For a reversible process the peak current is described by the Randles–Ševčik equation:

$$i_{pa} = knFA_{RS}C\sqrt{\frac{nFD}{RT}}\sqrt{v} \quad (1)$$

where i_{pa} is the anodic peak current (A); k is a dimensionless constant, 0.4463; n is the number of transferred electrons, that for ferrocene/ferrocenium redox couple is 1 electron; A_{RS} is the electrode area by Randles–Ševčik (cm^2); F is the Faraday constant, 96485.33212 C/mol; D is the diffusion coefficient in AN, 2.24×10^{-5} cm^2/s [32]; C is the bulk concentration of ferrocene, 1.00×10^{-6} mol/cm^3; ν is the voltage scan rate (V/s); R is the molar gas constant, 8.31446 J/(K mol) [33]; and T is the thermodynamic temperature, 298.15 K. A plot of i_{pa} versus $\sqrt{v}$ results in a straight line with slope (s_{RS}):

$$s_{RS} = knFC\sqrt{\frac{nFD}{RT}}A_{RS} \quad (2)$$

A_{RS} was calculated from s_{RS} obtained by a set of measurements to take into account the response at the different scan rate:

$$A_{RS} = \frac{s_{RS}\sqrt{RT}}{knFC\sqrt{nFD}} \quad (3)$$

After each set of scans varying ν, A_{RS} was evaluated and the solution was replaced. This procedure was repeated, and A_{RS} was measured 35 times before and after the MT.

Measurements by LSV Varying the Rotation Frequency of the SGE

LSV was adopted in this case. The SGE was used in rotation mode and linear scans of potential from 0 V to 0.85 V were carried out. The instrumental parameters, namely scan rate, step potential and interval time, were maintained at 13.3 mV/s, 4 mV and 0.3 s respectively.

Six values of rotation frequency were investigated: 500, 1000, 1500, 2000, 2500 and 3000 rpm. For each rotation frequency a voltammogram was recorded. The value of in-

terest was the limiting current obtained when the plateau is reached, as described by the Levich equation:

$$I = \frac{k' n F A_L \sqrt[3]{D^2}\, C \sqrt{\omega}}{\sqrt[6]{\nu_{AN}}} \quad (4)$$

where I is the limiting current (A); k' is a constant, 0.620 $1/\sqrt{\text{rad}}$; n is the number of transferred electrons, that for ferrocene/ferrocenium redox couple is 1 electron; A_L is the electrode area by Levich (cm^2); ω is the angular frequency of the electrode (rad/s, obtained by 1 rad/s = 1 rpm/(2π/60)); and ν_{AN} is the kinematic viscosity of AN, 4.484000 × 10^{-3} cm^2/s. A plot of I as a function of $\sqrt{\omega}$ results in a straight line with slope (s_L):

$$s_L = \frac{k' n F A_L \sqrt[3]{D^2}\, C}{\sqrt[6]{\nu_{AN}}} \quad (5)$$

A_L was calculated from s_L obtained by a set of measurements to take into account the response at the different rotation frequency:

$$A_L = \frac{s_L \sqrt[6]{\nu_{AN}}}{k' n F C \sqrt[3]{D^2}}\,. \quad (6)$$

After each set of scans varying ω, A_L was evaluated and the solution was replaced. This procedure was repeated, and A_L was estimated 35 times before and after the MT.

2.2.2. SEM Analysis

An Inspect F SEM located at NanoFacility Piemonte, supported by Compagnia di San Paolo, at Istituto Nazionale di Ricerca Metrologica, INRiM, was employed in order to take frontal view images of the electrode area, from which the geometric area was determined. The instrument was previously calibrated with different reference standards for length.

With an image manipulation program, the part of inert insulation of the SGE was erased from the SEM image. Wolfram Mathematica was used for the image data processing: the conversion from a grayscale to a binary scale, the counting of the relationship between black pixels and total pixels, and the scaling of the relationship taking into account the image scale. Three images were acquired and processed before and after the MT. The mean of three values obtained by SEM investigations was named A_{SEM}.

2.3. Determination of the Exposed Surface of the SGE

CV in an unstirred 0.5 M solution of H_2SO_4 was used to investigate the exposed surface, S, of the SGE [34], which is the surface given by the sites able to react with an analyte. The potential was varied linearly from 0 to 1.5 V and back to 0 V 10 times, keeping the step potential at 0.00244 V to obtain a scan rate of 0.1 V/s. The voltammograms were recorded. S was evaluated on the base of the following equation [35]:

$$S = \frac{\int i_{pc} dE}{400\ \mu C/cm^2} \quad (7)$$

where S is expressed in cm^2, i_{pc} is the current intensity of the cathodic peak (A), $\int i_{pc}\, dE$ is the area included under the cathodic peak, and the constant at the denominator is an empirical value representing the theoretical charge associated with the reduction in the surface oxide monolayer per unit surface area of gold, as reported in the literature [35–37]. This procedure was repeated, and S was determined 15 times before and 15 times after the MT.

2.4. Mechanical Treatment

To evaluate the effect of the grooves of the SGE surface on the voltammetric response, their height was significantly reduced by carrying out the MT performed by a jeweler in Torino (Italy). He used different abrasive materials and brushes commonly adopted to polish noble metals-based surfaces. A specific tool to keep the SGE perpendicular to the abrasive brush was also used.

Commonly, before use, the SGEs undergo a polishing procedure. The electrode was polished sequentially with suspensions of 1, 0.3, and 0.05 µm alumina powder in HPW for 1 min, then SGE was immersed three times into ethanol and water alternatively to remove the remaining Al_2O_3 particles from the surface. This procedure was also applied to the SGE before the MT, but it was not sufficient to reduce the height of grooves (the SEM images are not reported).

2.5. Hg Detection with the SGE

The effect of the MT on the SGE was tested by detecting the voltammetric signal of Hg in a NaCl solution (see Section 2.1) by ASV. After 120 s of deposition at 0 V using a stirring rate of 1500 rpm, a scan was carried out by square wave (SW) in an unstirred solution, adopting the following parameters, previously optimized [18]: frequency, 150 Hz; initial potential, 0 V; final potential, 0.80 V; step potential, 0.0040 V; amplitude, 0.03 V; scan rate, 0.607 V/s.

The results obtained by 10 measurements of Hg peak height were evaluated before and after the MT.

3. Results

3.1. Determination of the Geometric Area of the SGE

For the determination of the geometric area of the SGE, voltammetric measurements on ferrocene and SEM images of the electrode were considered. Equations (3) and (6) were taken as mathematical models for the estimation of the expected values of A_{RS} and A_L, respectively. The obtained results of the quantities which affect the measurements were collected as independent observations under repeatability conditions. The experimental standard deviation of the mean for the obtained results, characterizing the uncertainty of the quantities that vary randomly, were used as the uncertainty of those quantities [38]. Concerning the A_{SEM} value, the mathematical model that estimates its expected value was the mean of the obtained results. The uncertainty of the value was estimated including the variability of the model applied by the software and the experimental standard deviation of the mean.

3.1.1. Voltammetric Measurements with Ferrocene

The oxidation of ferrocene to ferrocenium cation, $Fe(C_5H_5)_2^+$, was examined, due to its well-known reversible process of diffusion-controlled single electron transfer. Ferrocene commonly exhibits reversible redox behavior in all solvent media. For this work, AN was chosen because it enables a fast electron transfer due to a low uncompensated resistance effect compared to other media, for example dichloromethane [39]. The system AN/$TBAPF_6$ was adopted because the D of the ferrocene in it is well known from the literature. A high concentration of $TBAPF_6$ was added (in a ratio of 100:1 to ferrocene) to the solution in order to minimize the ohmic drop, to neglect the contribution of the redox couple to migration, and to ensure that the mass transport in the solution was exclusively by diffusion [40–42]. Moreover, since the resistance of the solution was really small, the current density was expected to be uniform across the disk and independent of the radial distance. More-

over, $TBAPF_6$ permits a fast reaction due to the interaction between the electrogenerated Fc^+ species and the PF_6^- anions [43,44].

The measurements were carried out keeping the potential under 0.85 V to avoid the oxidation of gold on the SGE surface, which occurs at 1.25 V, when we use chloride solutions. Before starting the measurements related to this study, an optimization process was developed. Different electrode cleaning procedures were tested:

- 0.06 M HCl solution with the WE rotated for 60 s at 0.6 V
- 0.5 M H_2SO_4 solution with the WE rotated for 5 cycles in the range between 0 and 1.5 V
- 0.1 M $HClO_4$/1.5 × 10^{-3} M NaCl/0.5 × 10^{-3} M $EDTANa_2$ solution with the WE rotated for 60 s at 0.6 V.

The latter was chosen since it demonstrated the best cleaning efficiency. The need to apply a deoxygenation of the solution before each determination was valued. Since no effects were observed, this step was not applied. Particular attention was paid to keep constant the setup of the measurements (solution preparation, cleaning procedure, electrodes conditions and temperature), in order to ensure the work always occurred with the same system. For this purpose, before starting the voltammetric measurements the profile obtained by 10 CV cycles in 0.5 M H_2SO_4 solution was used as a quality reference for the gold surface. If additional peaks appear in CV voltammogram, with respect to those expected for gold alone, they are probably due to the formation of oxide multilayers with gold in different oxidation states (Au0/AuI/AuIII) [34]. These layers cause a worse performance of the electrode. When this was the case, the cleaning procedure was applied again.

Determination of the Geometric Area of SGE by CV Varying the Scan Rate

First of all, it was necessary to develop a procedure for the measurement of i_{pa} values. In fact, at each scan rate, a shift between the first and subsequent scans was observed. This shift decreases when repeating the scans until stability is reached and the subsequent scans are overlapped. This last behavior indicates that the amounts of oxidized and reduced ferrocene are stable in the time of the measurement. The selected scan for the measurement of i_{pa} was the first one for which results completely overlapped with the following one. At the scan rate of 10 mV/s, the second scan was chosen. At the scan rates of 25 and 50 mV/s, the third scans were selected. At the scan rate of 100 mV/s, the fourth scan was selected. At the scan rates of 200, 300, 400 and 500 mV/s, the fifth scans were selected. Figure 1 shows an example of CV voltammogram at the scan rate of 500 mV/s. In this case, the fifth scan overlapped with the sixth one.

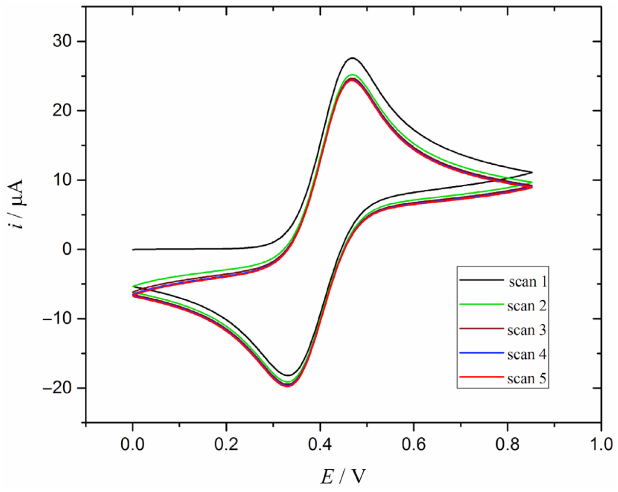


Figure 1. CV scans obtained at the scan rate of 500 mV/s.

For the SGE area determination, the scans at the eight selected scan rates form a set of CV voltammograms and summarize a measurement.

The 18th measurement is reported here as an example of all the steps used in the A_{RS} evaluation. Figure 2 shows the voltammograms at each scan rate. Table 1 reports the corresponding values of i_{pa} and Figure 3 points out the linear relationship between the latter and square root of scan rate. For the reported example s_{RS} was estimated as 1.165 μA/$\sqrt{}$(mV/s) by Equation (2) and the corresponding A_{RS} was 3.04 mm^2.

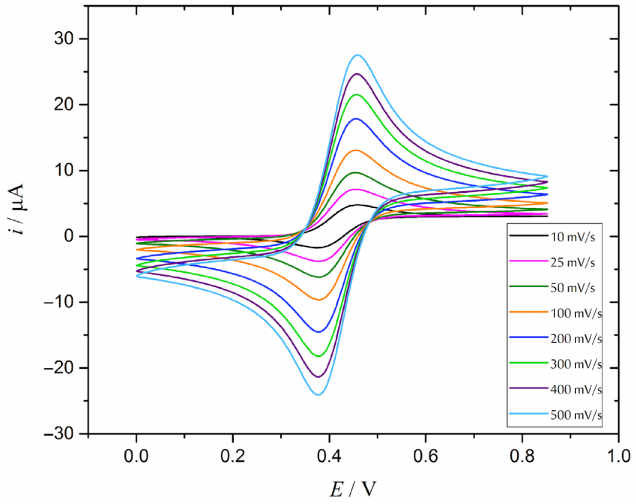


Figure 2. CV voltammograms obtained by a set of scans at the eight scan rates, 18th measurement before the MT.

Table 1. i_{pa} values obtained at each scan rate for the 18th measurement before the MT.

ν/mV/s	i_{pa}/μA
10	3.86
25	6.04
50	8.42
100	11.83
200	16.59
300	20.35
400	23.30
500	26.29

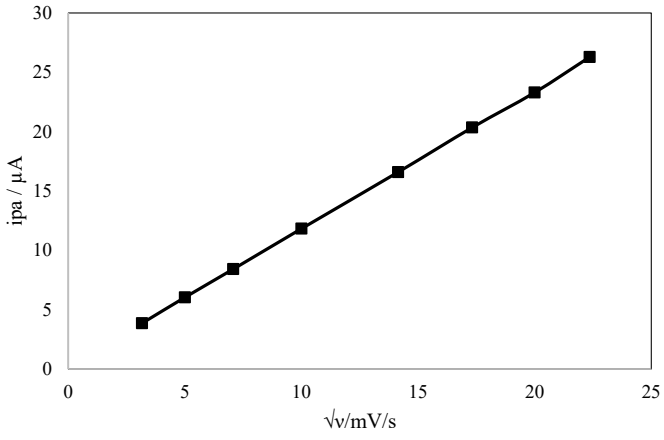


Figure 3. Graph of i_{pa} as a function of $\sqrt{\nu}$ for the 18th measurement before the MT.

A total of 35 values of A_{RS} were determined before the MT. The mean value was 2.93 mm^2, the standard deviation of the mean was 0.34 mm^2 and the relative standard

deviation (RSD%) was 11.5%. After the MT of the SGE surface, 35 measurements were repeated, and the correspondent A_{RS} values were obtained. The mean value was 2.67 mm^2, the standard deviation of the mean was 0.07 mm^2 and the RSD% was 2.5%. The single values of A_{RS} are reported in Table S1 (Supplementary Materials) and shown in Figure 4. The different repeatability obtained before and after the MT was not due to the variations in the temperatures and vibrations of the system since these were the same during all 70 measurements carried out.

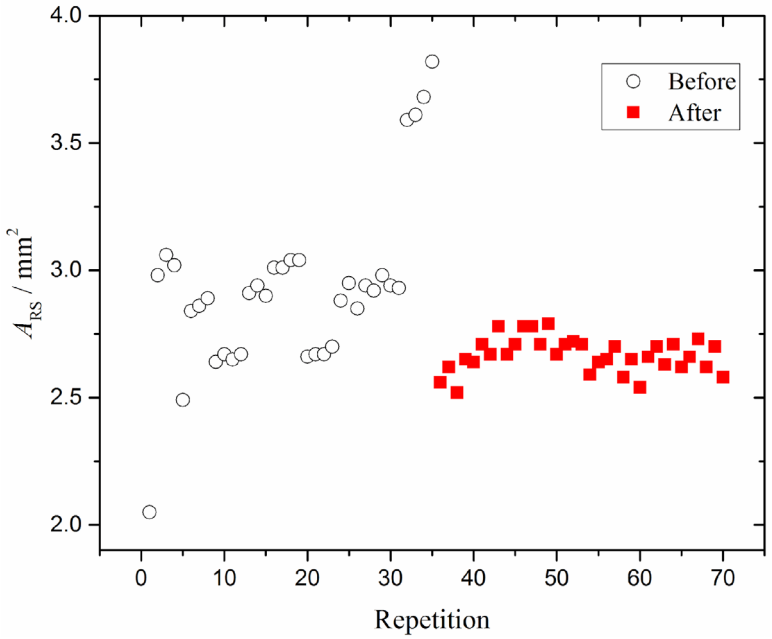


Figure 4. A_{RS} measurement repetitions before (O) and after (■) the MT.

The relevant variability of the A_{RS} data before the MT is not associated with the variation in the weighed amounts of ferrocene or $TBAPF_6$, to the package of reagents, or to the degradation of the samples; such variability can be ascribed to the height of the grooves. In fact, the solution penetrates randomly at different depths in the grooves, giving rise to a large range of possible results. After the MT instead, the grooves are significantly less deep. In this case, the solution penetrates for every measurement till the bottom of the grooves, causing a reduction in the range of possible results.

Reversibility Study and Diffusion-Control Conditions

Randles–Ševčik equation describes a reversible process in which transport occurs only by diffusion. In order to verify its applicability to this system, studies of reversibility were performed. CV measurements varying the scan rate were carried out in a stagnant solution. This method gives rise to characteristic diffusion-controlled peaks. The peaks increase when increasing the scan rate, since increasing the scan rate decreases the time for the diffusion layer to extend to the mass of the solution.

The CV voltammograms for ferrocene/ferrocenium redox couple are well known in the literature since they are typical for a reversible system [39].

(i) For a reversible system, the peak current ratio of the forward (cathodic peak, i_{pc}) and the reverse (or backward) (anodic peak, i_{pa}) scans is equal to unity (i_{pc}/i_{pa} = 1.0) and is independent of the scan rate. In the case of the 18th measurement, reported in Table 2, the ratio value was confirmed at each scan rate.

Table 2. Values of the relevant CV parameters at each scan rate for the 18th measurement before the MT.

ν/(mV/s)	$\sqrt{\frac{v}{\frac{mV}{s}}}$	E_{pa}/V	i_{pa}/μA	E_{pc}/V	i_{pc}/μA	ΔE/V	i_{pa}/i_{pc}	$E_{1/2}$/V
10	3.16	0.454	3.82	0.383	−3.67	0.071	−1.04	0.401
25	5.00	0.452	6.07	0.381	−5.72	0.071	−1.06	0.403
50	7.07	0.449	8.53	0.381	−8.15	0.068	−1.05	0.405
100	10.0	0.454	11.96	0.381	−11.57	0.073	−1.03	0.402
200	14.1	0.452	16.87	0.381	−16.61	0.071	−1.02	0.405
300	17.3	0.454	20.59	0.381	−20.38	0.073	−1.01	0.403
400	20.0	0.454	23.78	0.381	−23.56	0.073	−1.01	0.403
500	22.4	0.457	26.61	0.381	−26.4	0.076	−1.01	0.401

(ii) The peak potential spacing ($\Delta Ep = Epa - Epc$) for a fast, reversible, one electron transfer system is $\Delta Ep = 0.059$ V at 298 K. In this study, ΔEp varies from 0.068 to 0.076 V. The discrepancy from the value related to a reversible system can be attributed to the solution resistance.

(iii) For a reversible system $E_{1/2}$ (calculated as $Epa - \Delta Ep/2$) does not depend on the scan rate value [37]. In this study, this behavior is confirmed, as shown in Table 2.

(iv) In Figure 5, both the values of i_{pa}, and i_{pc} are reported as a function of the square root of the scan rate. In the case of a reversible system the same considerations can be applied to both slopes. Also in this case, the symmetry of the slopes can be observed. Thus, the procedure for the evaluation of s_{RS} can also be applied to the cathodic plot. In this study, A_{RS} was calculated from s_{RS}, on the base of i_{pa}, as commonly reported in the literature [45].

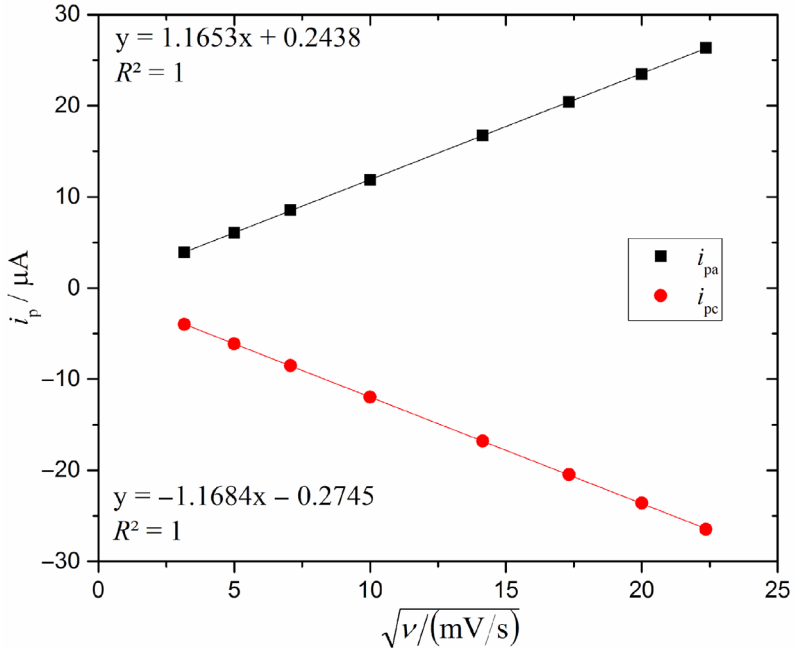


Figure 5. The anodic and the cathodic peak heights as a function of the square root of the scan rate for the 18th measurement before the MT.

(v) The plot of log i_{pa} versus log is reported in Figure 6 with a slope of 0.5 confirming the theoretical value for a purely diffusion-controlled current [46].

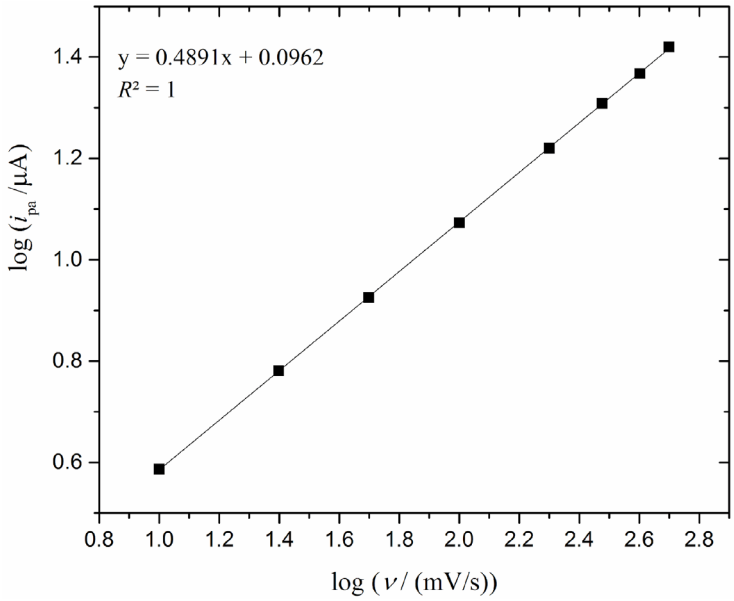


Figure 6. Graph of log i_{pa} values as a function of log for the 18th measurement before the MT.

(vi) In the case of a solid electrode in a stagnant solution, the diffuse layer, δ, is the region of the solution close to the electrode surface in which ions are mobile under the coupled influence of electrostatic forces and diffusion [47]. In CV the current passing through the electrode is limited by the diffusion of species to the electrode surface. This diffusion flux is influenced by the concentration gradient near the electrode and by the mobility of the species through the solution. When the scan rate rises, the concentration at the electrode surface increases, resulting in a higher current [48,49]. The diffusion layer at each point of the cyclic voltammogram gives rise to the characteristic peaks shape. For this study, the diffusive layer was calculated to be between 45 and 319 μm from $\delta \propto \sqrt{Dt}$ with D is the diffusion coefficient of the analyte in solution, and t is given by = ($E_{pa} - E_0$)/scan rate. Each value of A_{RS} was calculated from the slope obtained by a set of measurements to take into account the response at the different scan rates.

Determination of the Geometric Area of the SGE by LSV Varying the Electrode Rotation Frequency

In the voltammogram obtained by applying a linear voltage scan, a plateau of current is reached, which is named limiting current, I, and expressed in μA. In this study, due to the current fluctuation, the mean of six values of I, taken at six potential values > 0.83 V, was computed at each rotation frequency.

The most significant instrumental parameters, namely step potential, step time and scan rate, were changed in order to investigate their possible effects on the area measurements. The tested values were 2, 4 and 8 mV for the step potential; 0.60, 0.30 and 0.15 s for the step time; and 7, 13 and 27 mV/s for the scan rate. The correspondent voltammograms were recorded and no influence was observed.

Firstly, to check the repeatability of the response, five scans were performed at each rotation frequency and, since all the voltammograms were overlapped, in all the experiments the first one was selected.

Each A_L value (35 measurements) derives from a set of voltammograms obtained at the six rotation frequencies in the same sample solution. I was recorded in automatic mode. The 18th measurement is reported here as an example for all the steps adopted for A_L evaluation.

Figure 7 shows the voltammograms at each rotation frequency, Table 3 reports values of I varying $\sqrt{\omega}$ and Figure 8 points out the linear relationship between the two quantities.

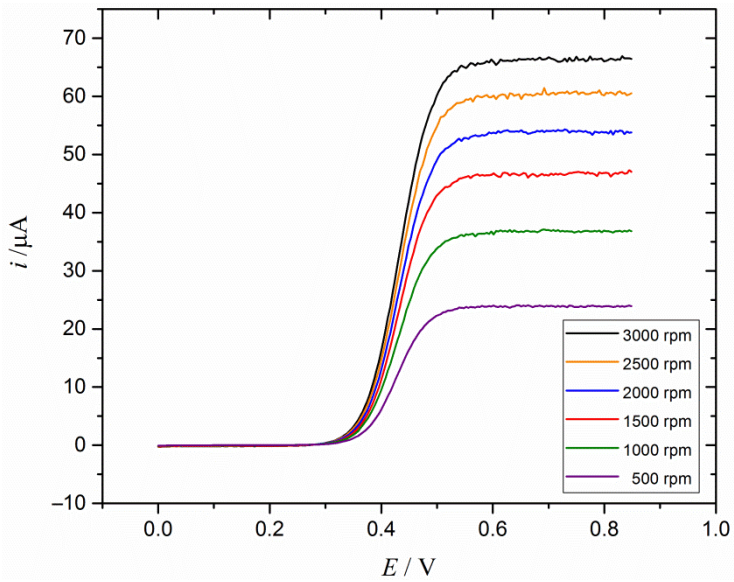


Figure 7. Set of LSV voltammograms obtained at each rotation speed for the 18th measurement before the MT.

Table 3. I value at each $\sqrt{\omega}$ for the 18th measurement before the MT.

$\sqrt{\frac{\omega}{\frac{rad}{s}}}$	***I*/μA**
7.236	23.92
10.233	36.83
12.533	46.94
14.472	53.86
16.180	60.50
17.725	66.55

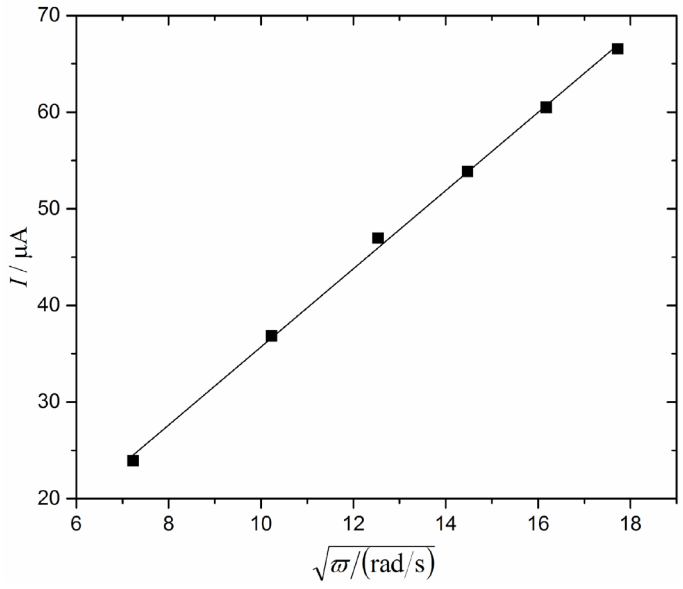


Figure 8. Graph of I as a function of $\sqrt{\omega}$ for the 18th measurement before the MT.

For the reported example, s_L was estimated as 4.046 μA/$\sqrt{}$(rad/s) considering Equation (5), and the corresponding A_L was 3.73 mm^2.

A total of 35 values of A_L were determined before the MT of the SGE surface. The mean value was 3.52 ± 0.37 mm^2. After the MT, the 35 measurements were repeated, and the corresponding A_L values were estimated. The mean value was 3.05 ± 0.10 mm^2. All the values of A_L are reported in Table S2 and shown in Figure 9. As previously observed for the CV approach, the variability of the A_L data remarkably decreases after the MT. The same comments are in force in this case.

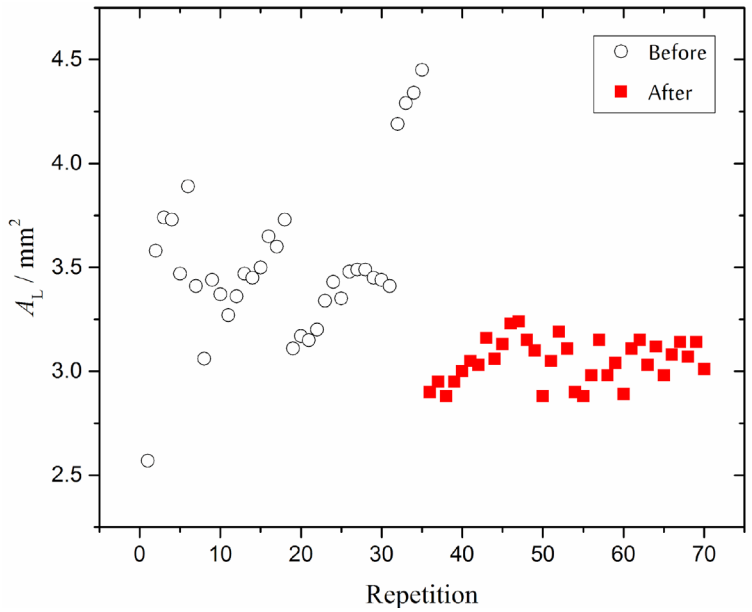


Figure 9. A_L measurement repetitions before (O) and after (■) the MT.

Diffusion Layer Thickness

The laminar flow at the SGE conveys a steady stream of material from the bulk solution to the electrode surface. While the bulk solution remains stirred by the induced rotation, the solution layer nearest to the electrode surface appears stagnant since it rotates with the electrode. Transport of analyte from the bulk solution into the stagnant layer occurs by convection. After the analyte enters the stagnant layer, it moves to the electrode surface by diffusion. Rapid solution flow ensures uniformity of composition. The constant transport of electroactive species across this diffusion layer creates a stable steady state [39]. The diffusion layer thickness is given by $\delta = 1.61\sqrt[3]{D}\ \sqrt[6]{\nu}\ /\sqrt{\omega}$, where D is the diffusion coefficient (cm^2/s), ω is the rotation frequency of the electrode (rad/s) and ν is the kinematic viscosity (cm^2/s). From the above equation, δ_0 results are 0.02547, 0.01801, 0.01470, 0.01273, 0.01139 and 0.01040 mm at the rotation frequencies of 500, 1000, 1500, 2000, 2500 and 3000 rpm, respectively. Thus, for this study, the minimum δ_0 result was about 10 µm at 3000 rpm. These results are in good agreement with the values of δ_0 reported in the literature for solid electrodes [50].

3.1.2. Morphological Characterization

SEM analyses were performed to investigate the surface of the SGE and to evaluate its geometric area. For the latter, images were taken at low magnification to contain the whole area (Figure S1).

In Figure 10, a SEM image of the surface of the SGE as received by the manufacturer was reported. It is possible to observe a long groove which forms a sort of spiral (also visible to the naked eye). This groove was created during the process of fabrication. Figure 11 show image of the SGE before the MT. In particular, shows part of the groove whose height was estimated at about 2 µm.

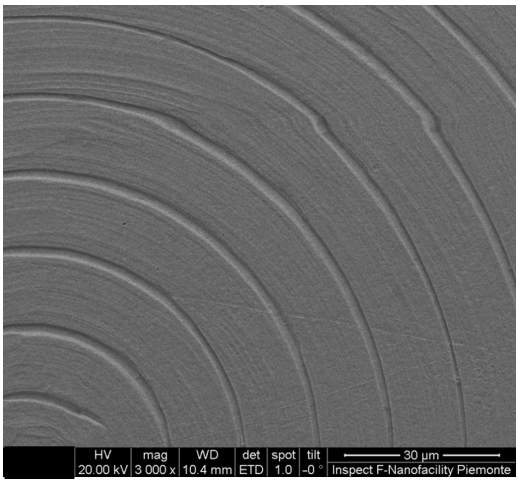


Figure 10. The grooves on the surface of the SGE as received from the producer.

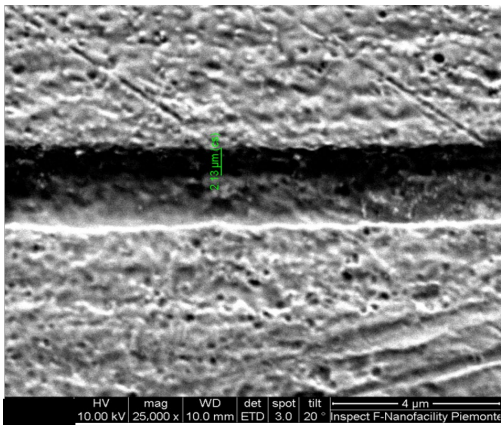


Figure 11. SEM image of the detail of the grooves present on the surface of the SGE as received from the producer.

Figure 12 show images of the SGE after the MT. It is possible to observe that the MT caused a reduction in the height of the grooves of ten times, from 2 µm to about 0.2 µm.

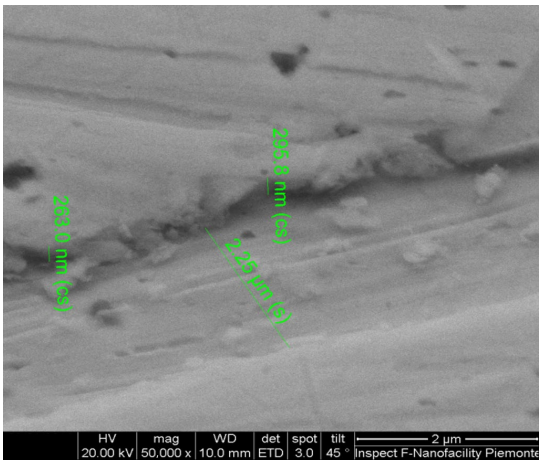


Figure 12. SEM image of a detail of the grooves present on the surface of the SGE after the MT.

With the aid of the calibrated reference length reported on the SEM images and of the Wolfram Mathematica 14.0 software, the geometric area of the SGE, A_{SEM}, was calculated. The mean value, calculated from the values obtained from three images of the SGE before the MT, was 3.20 ± 0.01 mm^2, while that obtained after was 3.23 ± 0.006 mm^2.

An uncertainty of 1%, associated with the variability of the model, was added, which includes also the variability of the number of pixels identified as the edge of the electrode. The uncertainty associated with the geometric area value was evaluated following the rule accepted at international level [38].

The repeatability values before and after the MT, given by the standard deviation of the mean and the uncertainty of the model, resulted in 0.03 mm^2. A_{SEM} values before and after the MT are not significantly different, as confirmed by *t*-test ($p < 0.05$). All the single values of A_{SEM} are reported in Table S3.

Calculation of the Extended Area

Before the MT on the SGE, a study was devoted to the evaluation of an "extended area", named A_{EX}, which includes both A_{SEM} and the area of the groove walls, A_{GW}. For the calculation, an approximation was made: instead of a unique long spiral, 66 concentric grooves were taken into account. The height of the grooves, *h*, the distance between grooves, a, the radius of the first groove, $r_{1°g}$, and the width of the grooves, *x*, were about 2.3 µm, 13.3 µm, 17.6 µm, 1.7 µm, respectively. A_{EX} was evaluated by $A_{EX} = A_{SEM} + A_{GW}$, considering $A_{GW} = \sum_{n=0}^{66} 2\pi h \left(2r_{1°g} + 2na + (2n+1)x\right)$. The resulting area was estimated as A_{EX} = 3.20 + 0.97 = 4.17 mm^2. After the MT, the grooves were reduced by about ten times (see Figure 12) and they were not observable to the naked eye anymore. In this case A_{GW} contribution was evaluated at 0.10 mm^2, and consequently A_{EX} = 3.23 + 0.10 = 3.33 mm^2.

3.1.3. Comparison of the Geometric Area Values

The electrode area reported in Equations (1) and (4) is commonly considered as the projection of the surface on a parallel plane. This geometric area approach is justified by the fact that for the considered voltammetric techniques the current is controlled by diffusion, rather than by reaction kinetics [30].

Table 4 and Figure 13 summarize the geometric area values obtained by voltammetry and SEM with corresponding error bars. A complete evaluation of the measurement uncertainty was not possible, because the potentiostat, which supplies the potential at specific scan rates and measures the current, was not calibrated for these quantities. Despite the results not taking into account the above-mentioned uncertainty contributions, it is observable from Figure 13 that the area values obtained by voltammetry are not consistent, both considering the values before and after the MT, and within the techniques, as confirmed by *t*-test ($p < 0.05$). This means that the ascertainment, on the basis of which the voltammetric techniques should involve the geometric area of the SGE, is at least questionable. It is generally accepted that, if the diffusion layer thickness at the electrode/solution interface is greater than the height of the surface promontories, these latter promontories do not affect the area estimations. In this study, the grooves on the SGE surface before the MT were about 2 µm height, substantially lower than the thickness of the diffusion layer, which exhibited a minimum thickness of about 10 µm. Thus, the irregularities of the surface should not have affected the geometric area involved in the voltammetric measurements.

Table 4. Results obtained by the three techniques considered for the geometric area (mm^2).

Geometric Area	A_{RS}		A_L		A_{SEM}	
	Before MT	**After MT**	**Before MT**	**After MT**	**Before MT**	**After MT**
Repetitions	35	35	35	35	3	3
Mean	2.93	2.67	3.52	3.05	3.2	3.23
Repeatability	0.06	0.01	0.06	0.02	0.03	0.03
RSD%	11.5	2.5	10.6	3.4	0.3	0.2

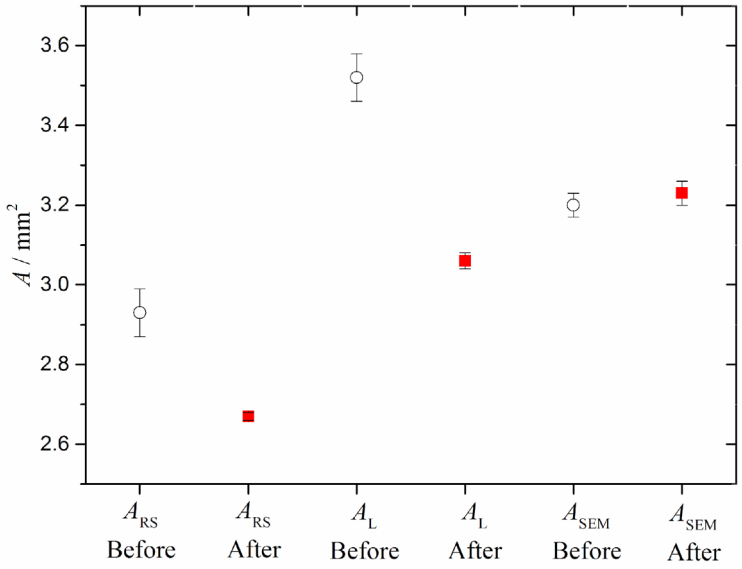


Figure 13. Geometric area values obtained by the voltammetry measurements and SEM analysis before the MT (O) and with the same techniques after the MT (■).

In addition, the decreasing of A_{RS} after the MT, is due to the effect of h on i_{pa} at different values of ν, as also observed by Parveen [51]; at high values of ν, i_{pa} is proportional to h, while at low values of ν, i_{pa} is not affected by h. Thus, after the MT s_{RS} as well as the correspondent area decreases.

A_L has to be considered differently: since the electrode rotates, the diffusion layer follows the variation in the rotation speed. Before the MT, A_L was larger than A_{SEM}. Two possible hypotheses can be made: (i) the solution penetrates up to a certain level of depth between the grooves, and the diffusion layer can perceive the largest area; (ii) the grooves behave like microelectrodes, for which radial diffusion also has to be taken into account. After the MT, A_L value is closer to A_{SEM} because the grooves are reduced and the diffusion layer perceives the geometric area.

A statistical comparison among the results, obtained by the different techniques, was also made using ANOVA (level of probability = 95%); the area values turned out to be significantly different to each other. Regarding the comparison between voltammetric and microscopy techniques, it is observable that after the MT A_L value is closer to A_{SEM} than A_{RS}.

Moreover, regarding the comparison between the two voltammetric techniques, LSV varying the electrode stirring rate is preferable with respect to CV varying the scan rate for the calculation of the electrode area because: (i) the rate of mass transport of reactants to a rotated surface is controlled accurately by fixing the various ω; (ii) I quickly achieves steady state values and it is independent of the potential scan rate; (iii) I is insensitive to incidental vibrations of the apparatus and erratic natural convection [21].

3.2. Exposed Surface of the SGE in H_2SO_4

Gold is easily oxidized and can absorb Cl^- or impurities from the solution, gradually reducing the number of active sites on the surface of the electrode. CV in acid solutions is commonly used in the pretreatment and in the daily activation step of gold electrodes, in order to maintain their surface activity and reproducibility [10]. In particular, the use of H_2SO_4 enables a structural reorganization of gold [10]. The information on the energy of the surface activation states [52,53] and the surface quality can be provided by a CV voltammogram.

This profile is considered as a "fingerprint" of the gold faces [35]. In fact, it includes the electrochemical double layer region, the formation of a monolayer of oxide (and its subsequent reduction), and the beginning of the reduction in protons (or of the solvent). CV in 0.5 M H_2SO_4 is adopted to estimate the amount of gold active sites on the electrode surface, which are the sites that react with the analyte. All these sites together can compose a type of area, which is here named exposed surface, *S*. The value of the theoretical charge associated with the reduction (cathodic peak at +0.90 V) of the surface oxide monolayer per unit of surface area of gold was taken from the literature [37] and is equal to 400 μC/cm^2 [54,55].

This technique is particularly used when gold-based layers are deposited on the electrode surface, in order to monitor the amount and the activation status of the gold coating [10,37]. In this case, the steady state is not achieved during the measurement, and the obtained surface value is reported as a function of empirical parameters.

It is important to remember that measurements by CV in H_2SO_4 are strongly dependent on the cleanliness of the electrode surface, the used glassware, and the purity of solvents and chemicals. If these conditions are not met, the resulting voltammograms are without significance [31].

In this study, the cyclic voltammogram obtained after 10 cycles (Figure 14) was used to determine the *S* of the SGE. The 10th cycle was chosen since the voltammograms obtained in the following ones overlapped.

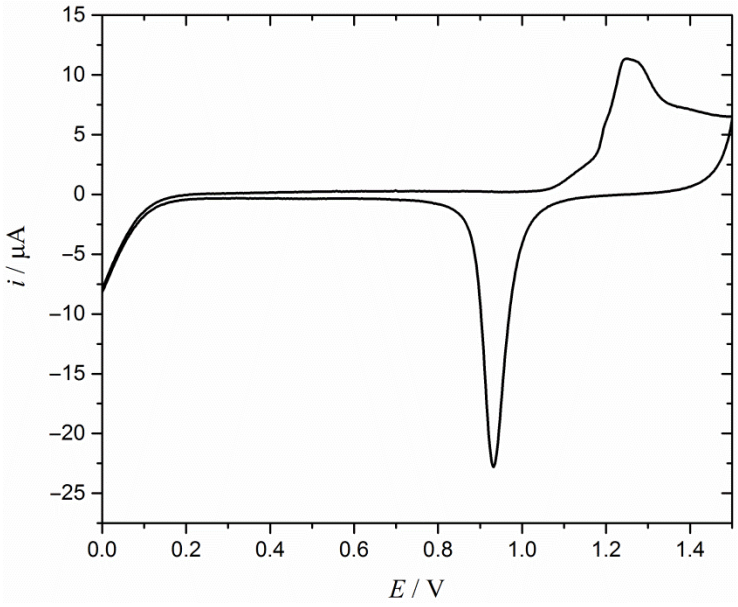


Figure 14. CV voltammogram of the SGE recorded in H_2SO_4 solution, used as a quality reference.

CV measurements in H_2SO_4 were performed 15 times before and after the MT of the SGE. Table 5 reports the final results of *S*, while the values are reported in Table S4.

Table 5. S values (mm^2) obtained by CV in H_2SO_4 before and after the MT.

Exposed Area	***S***	
	Before MT	**After MT**
Repetitions	15	15
Mean	4.46	4.86
Repeatability	0.06	0.12
RSD%	5.5	9.6

S and its RSD% slightly increase after the MT. This behavior probably derives from the mechanical removal of the oxide layers given by the MT, which takes out the adsorbed impurities on the surface and renews the sites. Moreover, a decreasing trend was observed within the values of i_{pc} after the MT. In the first measurements after the MT, i_{pc} was very high, then a decreasing trend was observed until it stabilized after at the seventh measurement, reaching the same value as in voltammogram reported in Figure 14. This behavior explains the high value of RSD%.

3.3. Effect of the Mechanical Treatment on Hg Detection by ASV

The detection of Hg in different types of matrices by ASV is one of the most important applications of the SGE. For this reason and in order to verify the effect of MT on the analytical response, Hg detections by ASV were performed on the SGE as received from the producer and after the MT. As an example, the voltammogram obtained analyzing the 1 μg/L Hg solution is shown in Figure S2. The voltammogram was previously corrected for the blank signal. It is possible to see the typical peak associated with the Hg oxidation at the potential of + 0.58 V.

Table S5 reports the 10 anodic current values, i_a, measured. Before the MT, the mean value, the standard deviation of the mean and the RSD% were 0.81 μA, 0.05 μA and 6.2%, respectively. After, the corresponding values were 1.97 μA, 0.05 μA and 2.3%, respectively.

It is possible to observe that after the MT (i) i_a values increased, despite the same amount of Hg reacted, and (ii) the repeatability of the measurements improved [27]. These results show the need to check the presence of the grooves on the SGE surface and possibly to remove them since they affect the performance of the electrode.

4. Conclusions

The Randles–Ševčik and Levich approaches produced geometric-area estimates that were not mutually consistent and did not reliably match SEM-based measurements on commercial solid-gold electrodes. Although the manufacturing grooves (2 μm) are smaller than the expected diffusion layer (45–319 μm) and should not, in principle, affect geometric area, the experimental results show that this assumption is not always valid. The grooved surface behaves more like an array of microelectrodes, altering mass transport and compromising area determination, especially after strong mechanical modification. A drastic mechanical polishing treatment reduced groove height (2 μm to 0.2 μm), improved the repeatability of area measurements (RSD from 11% to 3%), and made the Levich-derived area closely agree with the SEM area. The treatment also removed aged oxide layers and impurities, restoring active gold sites. Between the two voltammetric methods, LSV at controlled rotation rates is preferable for area evaluation because mass transport can be precisely tuned and steady-state currents are largely independent of scan rate and less affected by convection or vibrations. The practical benefit of polishing was confirmed by anodic stripping voltammetry for Hg: the stripping peak current more than doubled and precision improved.

Supplementary Materials: The following supporting information can be downloaded at: https://www.mdpi.com/article/10.3390/analytica7010016/s1, Figure S1. SEM image of whole area of electrode; Figure S2. Voltammogram obtained analyzing the 1 μg/L Hg solution with the SGE as received by the producer; Table S1. Values of ARS obtained before and after the MT; Table S2. Values of AL obtained before and after the MT; Table S3. Values of ASEM obtained before and after the MT; Table S4. Values of S obtained before and after the MT; Table S5. Values of ia measured by ASV in a sample with 1 μg/L of Hg before and after the MT; Explanation of different areas; Mechanical Treatment performed by a jeweller.

Author Contributions: Conceptualization, P.I., A.G. and F.D.; methodology, G.R.; validation, E.O. and G.R.; formal analysis, G.R.; investigation, P.I.; resources, A.G.; data curation, M.M. and L.M.; writing—original draft preparation, P.I.; writing—review and editing, F.D. and O.A.; visualization, A.G.; supervision, A.G. and F.D.; project administration, A.G.; funding acquisition, A.G. All authors have read and agreed to the published version of the manuscript.

Funding: This research received no external funding.

Data Availability Statement: Data is contained within the article or Supplementary Materials.

Conflicts of Interest: The authors declare no conflicts of interest.

References

1. Piech, R.; Paczosa-Bator, B. New Adsorptive Stripping Determination of ATP with Thorium(IV) on Renewable Silver Amalgam Film Electrode. *Int. J. Electrochem. Sci.* **2014**, *9*, 4287–4296. [CrossRef]
2. Illuminati, S.; Truzzi, C.; Annibaldi, A.; Migliarini, B.; Carnevali, O.; Scarponi, G. Cadmium Bioaccumulation and Metallothionein Induction in the Liver of the Antarctic Teleost *Trematomus bernacchii* during an on-Site Short-Term Exposure to the Metal via Seawater. *Toxicol. Environ. Chem.* **2010**, *92*, 617–640. [CrossRef]
3. Inaudi, P.; Abollino, O.; Argenziano, M.; Malandrino, M.; Guiot, C.; Bertinetti, S.; Favilli, L.; Giacomino, A. Advancements in Portable Voltammetry: A Promising Approach for Iron Speciation Analysis. *Molecules* **2023**, *28*, 7404. [CrossRef] [PubMed]
4. Martín-Yerga, D.; González-García, M.B.; Costa-García, A. Electrochemical Determination of Mercury: A Review. *Talanta* **2013**, *116*, 1091–1104. [CrossRef]
5. Hidalgo, J.; Turdean, G.L.; Vilasó-Cadre, J.E.; Galambos, I.; Reyes-Domínguez, I.A.; Hidalgo, L.; Ignat, N.; Llanos-Lizcano, R. An Optimized Chemically Modified Electrode Based on Copper Oxide Nanorods for the Quantification of Chemical Oxygen Demand in Wastewater. *Inorg. Chem. Commun.* **2025**, *179*, 114848. [CrossRef]
6. Hidalgo, J.S.; Mukhtar, S.; Uddin, I.; Horváth, O.; Galambos, I.; Gábor, M.; Hidalgo, L.; Vilasó-Cadre, J.E.; Reyes-Domínguez, I.A.; Lakkakula, J. Green Silver–Bioinspired Nanoparticles Used as an Electrochemical Sensor—An Efficient and Simple Method for the Determination of Glyphosate in Surface Water Samples. *Ionics* **2025**, *32*, 1157–1173. [CrossRef]
7. Brainina, K.Z.; Stozhko, N.Y.; Shalygina, Z.V. Surface Microreliefs and Voltage–Current Characteristics of Gold Electrodes and Modified Thick-Film Graphite-Containing Electrodes. *J. Anal. Chem.* **2004**, *59*, 753–759. [CrossRef]
8. Korolczuk, M.; Ochab, M.; Gęca, I. Anodic Stripping Voltammetric Procedure of Thallium(I) Determination by Means of a Bismuth-Plated Gold-Based Microelectrode Array. *Sensors* **2024**, *24*, 1206. [CrossRef]
9. Inaudi, P.; Mondino, E.; Abollino, O.; Malandrino, M.; Argenziano, M.; Favilli, L.; Boschini, R.; Giacomino, A. On-Site Determination of Methylmercury by Coupling Solid-Phase Extraction and Voltammetry. *Molecules* **2022**, *27*, 3178. [CrossRef]
10. Inaudi, P.; Esposito, C.; Malandrino, M.; Favilli, L.; Giacomino, A.; Abollino, O. Development of a Portable Method for Monitoring and Speciation of Arsenic in Aquatic Systems by Anodic Stripping Voltammetry: Applications to Real Samples. *Talanta* **2025**, *291*, 127880. [CrossRef]
11. Ermakov, S.S.; Borzhitskaya, A.V.; Moskvin, L.N. Electrochemical Polishing of the Surface of a Gold Electrode and Its Effect on the Sensitivity of the Stripping Voltammetric Determination of Mercury(II). *J. Anal. Chem.* **2001**, *56*, 542–545. [CrossRef]
12. Khor, C.K.; Denker, S.; Ignaszak, A. Surface Analysis of Metrohm BT220 Screen-Printed Electrodes through Electrochemical Techniques: Importance of Pretreatment. *Front. Chem.* **2025**, *13*, 1602365. [CrossRef] [PubMed]
13. Bonfil, Y.; Brand, M.; Kirowa-Eisner, E. Determination of Mercury and Copper in Waste Water by Anodic-Stripping Voltammetry at the Gold Electrode. *Rev. Anal. Chem.* **2000**, *19*, 201–216. [CrossRef]
14. Celesti, C.; Giofrè, S.V.; Espro, C.; Legnani, L.; Neri, G.; Iannazzo, D. Modified Gold Screen-Printed Electrodes for the Determination of Heavy Metals. *Sensors* **2024**, *24*, 4935. [CrossRef]
15. Augelli, M.A.; Munoz, R.A.A.; Richter, E.M.; Cantagallo, M.I.; Angnes, L. Analytical Procedure for Total Mercury Determination in Fishes and Shrimps by Chronopotentiometric Stripping Analysis at Gold Film Electrodes after Microwave Digestion. *Food Chem.* **2007**, *101*, 579–584. [CrossRef]
16. Giacomino, A.; Ruo Redda, A.; Caligiuri, R.; Inaudi, P.; Squadrone, S.; Abete, M.C.; Abollino, O.; Morandi, S.; Conca, E.; Malandrino, M. Development of an Easy Portable Procedure for On-Site Determination of Mercury and Methylmercury. *Food Chem.* **2020**, *342*, 128347. [CrossRef]
17. Trasatti, S.; Petrii, O.A. Real Surface Area Measurements in Electrochemistry. *J. Electroanal. Chem.* **1992**, *327*, 353–376. [CrossRef]
18. Sing, K.S.W. Reporting Physisorption Data for Gas/Solid Systems with Special Reference to the Determination of Surface Area and Porosity (Recommendations 1984). *Pure Appl. Chem.* **1985**, *57*, 603–619. [CrossRef]
19. Tang, P.; Chew, N.Y.K.; Chan, H.-K.; Raper, J.A. Limitation of Determination of Surface Fractal Dimension Using N_2 Adsorption Isotherms and Modified Frenkel−Halsey−Hill Theory. *Langmuir* **2003**, *19*, 2632–2638. [CrossRef]

20. Feng, K.; Liu, G.; Zhang, Z.; Liu, H.; Lv, R.; Wang, X.; Chang, P.; Lin, J.; Barakos, G. Fractal Strategy for Improving Characterization of N2 Adsorption–Desorption in Mesopores. *Fractal Fract.* **2024**, *8*, 617. [CrossRef]
21. Hanaor, D.A.H.; Ghadiri, M.; Chrzanowski, W.; Gan, Y. Scalable Surface Area Characterization by Electrokinetic Analysis of Complex Anion Adsorption. *Langmuir* **2014**, *30*, 15143–15152. [CrossRef]
22. Go, J.-Y.; Pyun, S.-I.; Hahn, Y.-D. A Study on Ionic Diffusion towards Self-Affine Fractal Electrode by Cyclic Voltammetry and Atomic Force Microscopy. *J. Electroanal. Chem.* **2003**, *549*, 49–59. [CrossRef]
23. Dobrescu, G.; Georgescu-State, R.; Papa, F.; Staden, J.F.v.; State, R.N. Fractal Properties of Composite-Modified Carbon Paste Electrodes—A Comparison between SEM and CV Fractal Analysis. *Fractal Fract.* **2024**, *8*, 205. [CrossRef]
24. Altomonte, S.; Falciola, L.; Mussini, P.R.; Trasatti, S.; Gennaro, A.; Isse, A.A. Real Surface Area of Catalytic Silver Electrodes: The "Subjective" Molecular Probe Perspective. *Russ. J. Electrochem.* **2008**, *44*, 104–112. [CrossRef]
25. Martínez-Hincapié, R.; Wegner, J.; Anwar, M.U.; Raza-Khan, A.; Franzka, S.; Kleszczynski, S.; Čolić, V. The Determination of the Electrochemically Active Surface Area and Its Effects on the Electrocatalytic Properties of Structured Nickel Electrodes Produced by Additive Manufacturing. *Electrochim. Acta* **2024**, *476*, 143663. [CrossRef]
26. Bard, A.J.; Faulkner, L.R.; White, H.S. *Electrochemical Methods: Fundamentals and Applications*, 3rd ed.; Wiley: Hoboken, NJ, USA, 2022; ISBN 978-1-119-33406-4.
27. Ngamchuea, K.; Eloul, S.; Tschulik, K.; Compton, R.G. Planar Diffusion to Macro Disc Electrodes—What Electrode Size Is Required for the Cottrell and Randles-Sevcik Equations to Apply Quantitatively? *J. Solid. State Electrochem.* **2014**, *18*, 3251–3257. [CrossRef]
28. Levič, V.G.; Levič, V.G. *Physicochemical Hydrodynamics*, 2nd ed.; Prentice Hall international series in the physical and chemical engineering sciences; Prentice-Hall: Englewood Cliffs, NJ, USA, 1962; ISBN 978-0-13-674440-5.
29. Ward, K.R.; Gara, M.; Lawrence, N.S.; Hartshorne, R.S.; Compton, R.G. Nanoparticle Modified Electrodes Can Show an Apparent Increase in Electrode Kinetics Due Solely to Altered Surface Geometry: The Effective Electrochemical Rate Constant for Non-Flat and Non-Uniform Electrode Surfaces. *J. Electroanal. Chem.* **2013**, *695*, 1–9. [CrossRef]
30. Jiang, P.N. (Ed.) *Electroanalytical Chemistry Research Developments*; Nova Science Publishers: New York, NY, USA, 2007; ISBN 978-1-60021-927-6.
31. Gira, M.J.; Tkacz, K.P.; Hampton, J.R. Physical and Electrochemical Area Determination of Electrodeposited Ni, Co, and NiCo Thin Films. *Nano Converg.* **2016**, *3*, 6. [CrossRef]
32. Wang, Y.; Rogers, E.I.; Compton, R.G. The Measurement of the Diffusion Coefficients of Ferrocene and Ferrocenium and Their Temperature Dependence in Acetonitrile Using Double Potential Step Microdisk Electrode Chronoamperometry. *J. Electroanal. Chem.* **2010**, *648*, 15–19. [CrossRef]
33. Newell, D.B.; Cabiati, F.; Fischer, J.; Fujii, K.; Karshenboim, S.G.; Margolis, H.S.; De Mirandés, E.; Mohr, P.J.; Nez, F.; Pachucki, K.; et al. The CODATA 2017 Values of h, e, k, and N_A for the Revision of the SI. *Metrologia* **2018**, *55*, L13–L16. [CrossRef]
34. Burke, L.D.; Moran, J.M.; Nugent, P.F. Cyclic Voltammetry Responses of Metastable Gold Electrodes in Aqueous Media. *J. Solid State Electrochem.* **2003**, *7*, 529–538. [CrossRef]
35. Govindhan, M.; Amiri, M.; Chen, A. Au Nanoparticle/Graphene Nanocomposite as a Platform for the Sensitive Detection of NADH in Human Urine. *Biosens. Bioelectron.* **2015**, *66*, 474–480. [CrossRef]
36. Hamelin, A. Cyclic Voltammetry at Gold Single-Crystal Surfaces. Part 1. Behaviour at Low-Index Faces. *J. Electroanal. Chem.* **1996**, *407*, 1–11. [CrossRef]
37. Dai, X.; Nekrassova, O.; Hyde, M.E.; Compton, R.G. Anodic Stripping Voltammetry of Arsenic(III) Using Gold Nanoparticle-Modified Electrodes. *Anal. Chem.* **2004**, *76*, 5924–5929. [CrossRef] [PubMed]
38. Evaluation of Measurement Data: Guide to the Expression of Uncertainty in Measurement. JCGM 2008. Available online: http://www.bipm.org/utils/common/documents/jcgm/JCGM_100_2008_E.pdf (accessed on 10 July 2025).
39. Tsierkezos, N.G. Cyclic Voltammetric Studies of Ferrocene in Nonaqueous Solvents in the Temperature Range from 248.15 to 298.15 K. *J. Solut. Chem.* **2007**, *36*, 289–302. [CrossRef]
40. Pajkossy, T.; Nyikos, L. Diffusion to Fractal Surfaces—III. Linear Sweep and Cyclic Voltammograms. *Electrochim. Acta* **1989**, *34*, 181–186. [CrossRef]
41. Dickinson, E.J.F.; Limon-Petersen, J.G.; Rees, N.V.; Compton, R.G. How Much Supporting Electrolyte Is Required to Make a Cyclic Voltammetry Experiment Quantitatively "Diffusional"? A Theoretical and Experimental Investigation. *J. Phys. Chem. C* **2009**, *113*, 11157–11171. [CrossRef]
42. Tichter, T.; Tichter, A.; Andrae, D.; Roth, C. Simulating Cyclic Voltammetry at Rough Electrodes by the Digital-Simulation–Deconvolution–Convolution Algorithm. *Electrochim. Acta* **2024**, *508*, 145175. [CrossRef]
43. Yang, E.S.; Chan, M.-S.; Wahl, A.C. Electron Exchange between Ferrocene and Ferrocenium Ion. Effects of Solvent and of Ring Substitution on the Rate. *J. Phys. Chem.* **1980**, *84*, 3094–3099. [CrossRef]
44. Fabbrizzi, L. The Ferrocenium/Ferrocene Couple: A Versatile Redox Switch. *ChemTexts* **2020**, *6*, 22. [CrossRef]

45. Neghmouche, N.S.; Khelef, A.; Lanez, T. Investigation of Diffusion of Ferrocene and Ferricenium in Aqueous and Organic Medium Using Voltammetry Techniques. *Res. J. Pharm. Biol. Chem. Sci.* **2010**, *1*, 76–82.
46. Ngai, K.S.; Tan, W.T.; Zainal, Z.; Zawawi, R.M.; Zidan, M. Voltammetry Detection of Ascorbic Acid at Glassy Carbon Electrode Modified by Single-Walled Carbon Nanotube/Zinc Oxide. *Int. J. Electrochem. Sci.* **2013**, *8*, 10557–10567. [CrossRef]
47. Wang, J. *Analytical Electrochemistry*, 2nd ed.; Wiley-VCH: New York, NY, USA; Weinheim, Germany, 2000; ISBN 978-0-471-28272-3.
48. Abdelsalam, M.E.; Denuault, G.; Baldo, M.A.; Bragato, C.; Daniele, S. Detection of Hydroxide Ions in Aqueous Solutions by Steady-State Voltammetry. *Electroanalysis* **2001**, *13*, 289–294. [CrossRef]
49. Monteiro, M.C.O.; Jacobse, L.; Touzalin, T.; Koper, M.T.M. Mediator-Free SECM for Probing the Diffusion Layer pH with Functionalized Gold Ultramicroelectrodes. *Anal. Chem.* **2020**, *92*, 2237–2243. [CrossRef]
50. McNaught, A.D.; Wilkinson, A.; International Union of Pure and Applied Chemistry (Eds.) *Compendium of Chemical Terminology: IUPAC Recommendations*, 2nd ed.; Blackwell Science: Oxford, UK; Malden, MA, USA, 1997; ISBN 978-0-86542-684-9.
51. Parveen; Kant, R. Theory for Staircase Voltammetry and Linear Scan Voltammetry on Fractal Electrodes: Emergence of Anomalous Randles–Sevik Behavior. *Electrochim. Acta* **2013**, *111*, 223–233. [CrossRef]
52. Hamelin, A.; Martins, A.M. Cyclic Voltammetry at Gold Single-Crystal Surfaces. Part 2. Behaviour of High-Index Faces. *J. Electroanal. Chem.* **1996**, *407*, 13–21. [CrossRef]
53. Chico-Mesa, L.; Rodes, A.; Arán-Ais, R.M.; Herrero, E. Insights into Catalytic Activity and Selectivity of 5-Hydroxymethylfurfural Oxidation on Gold Single-Crystal Electrodes. *Nat. Commun.* **2025**, *16*, 3349. [CrossRef]
54. Angerstein-Kozlowska, H.; Conway, B.E.; Hamelin, A.; Stoicoviciu, L. Elementary Steps of Electrochemical Oxidation of Single-Crystal Planes of Au Part II. A Chemical and Structural Basis of Oxidation of the (111) Plane. *J. Electroanal. Chem. Interfacial Electrochem.* **1987**, *228*, 429–453. [CrossRef]
55. Behjati, S.; Koper, M.T.M. In Situ STM Study of Roughening of Au(111) Single-Crystal Electrode in Sulfuric Acid Solution during Oxidation–Reduction Cycles. *J. Phys. Chem. C* **2024**, *128*, 19024–19034. [CrossRef]

Disclaimer/Publisher's Note: The statements, opinions and data contained in all publications are solely those of the individual author(s) and contributor(s) and not of MDPI and/or the editor(s). MDPI and/or the editor(s) disclaim responsibility for any injury to people or property resulting from any ideas, methods, instructions or products referred to in the content.